Article

Polyfunctional Inorganic–Organic Hybrid Materials: An Unusual Kind of NLO Active Layered Mixed Metal Oxalates with Tunable Magnetic Properties and Very Large Second Harmonic Generation

Elena Cariati, Roberto Macchi, Dominique Roberto, Renato Ugo, Simona Galli, Nicola Casati, Piero Macchi, Angelo Sironi, Lapo Bogani, Andrea Caneschi, and Dante Gatteschi

J. Am. Chem. Soc., **2007**, 129 (30), 9410-9420• DOI: 10.1021/ja0710712 • Publication Date (Web): 07 July 2007

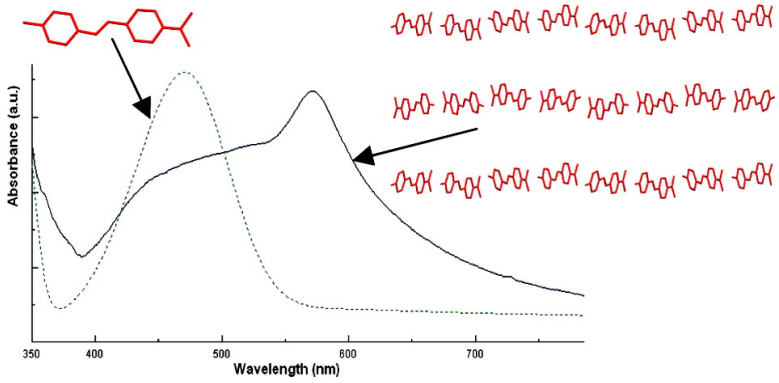

More About This Article

Additional resources and features associated with this article are available within the HTML version:

- Supporting Information
- Links to the 9 articles that cite this article, as of the time of this article download
- Access to high resolution figures
- Links to articles and content related to this article
- Copyright permission to reproduce figures and/or text from this article

View the Full Text HTML

J|A|C|S
ARTICLES
Published on Web 07/07/2007

Polyfunctional Inorganic−Organic Hybrid Materials: An Unusual Kind of NLO Active Layered Mixed Metal Oxalates with Tunable Magnetic Properties and Very Large Second Harmonic Generation

Elena Cariati,*,† Roberto Macchi,† Dominique Roberto,† Renato Ugo,† Simona Galli,‡ Nicola Casati,§ Piero Macchi,*,§ Angelo Sironi,§ Lapo Bogani,|| Andrea Caneschi,|| and Dante Gatteschi*,||

Contribution from the Dipartimento di Chimica Inorganica, Metallorganica e Analitica, Università di Milano, Centro CIMAINA, UdR di Milano INSTM and Centro ISTM-CNR, Via Venezian 21, 20133Milano, Italy, Dipartimento di Scienze Chimiche e Ambientali, Università dell'Insubria, Via Valleggio 11, 22100 Como, Italy, Dipartimento di Chimica Strutturale e Stereochimica Inorganica and Centro ISTM-CNR, via Venezian 21, 20133 Milano Italy, and Dipartimento di Chimica Università di Firenze and UdR di Firenze INSTM, via della Lastruccia 3, 50019 Sesto Fiorentino (FI), Italy

Received February 21, 2007; Revised Manuscript Received May 28, 2007; E-mail: elena.cariati@unimi.it; piero.macchi@unimi.it; dante.gatteschi@unifi.it

Abstract: Mixed M(II)/M(III) metal oxalates, as "stripes" connected through strong hydrogen bonding by *para*-dimethylaminobenzaldeide (DAMBA) and water, form an organic−inorganic 2D network that enables segregation in layers of the cationic organic NLO-phore *trans*-4-(4-dimethylaminostyryl)-1-methylpyridinium, [$DAMS^+$]. The crystalline hybrid materials obtained have the general formula $[DAMS]_4[M_2M'(C_2O_4)_6]\cdot 2DAMBA\cdot 2H_2O$ (M = Rh, Fe, Cr; M′ = Mn, Zn), and their overall three-dimensional packing is non-centrosymmetric and polar, therefore suitable for second harmonic generation (SHG). All the compounds investigated are characterized by an exceptional SHG activity, due both to the large molecular quadratic hyperpolarizability of [$DAMS^+$] and to the efficiency of the crystalline network which organizes [$DAMS^+$] into head-to-tail arranged J-type aggregates. The tunability of the pairs of metal ions allows exploiting also the magnetic functionality of the materials. Examples containing *antiferro*-, *ferro*-, and *ferri-magnetic* interactions (mediated by oxalato bridges) are obtained by coupling proper M(III) ions (Fe, Cr, Rh) with M(II) (Mn, Zn). This shed light on the role of weak next-nearest-neighbor interactions and main nearest-neighbor couplings along "stripes" of mixed M(II)/M(III) metal oxalates of the organic−inorganic 2D network, thus suggesting that these hybrid materials may display isotropic 1D magnetic properties along the mixed M(II)/M(III) metal oxalates "stripes".

Introduction

In the past few years, inorganic−organic hybrid crystalline materials with interesting electrical, magnetic, and nonlinear optical (NLO) properties have attracted the attention of the material science community,[1] in particular the appealing poly-functional hybrids.[2] The macroscopic functionalities of the latter can be originated by the combination of each individual component properties or by cooperative effects produced by a specific structural assembling. The advantage of resorting, at least in part, to molecular species of known properties prompts us to rationalize the engineering of the final material, thus allowing a tunability of the desired properties. In fact, the main purpose of the current research is to find the proper synergy between the two subsystems (organic and inorganic), each of which should contribute to retain (if not enhance) the other's property in an extended crystalline framework.

Within this wide new field, the coupling of magnetic and nonlinear optical properties is quite attractive[3] but yet largely unexplored. In particular, applications of combined electro-optic and magnetic materials have not received adequate attention, so far.

In hybrid materials, the most usual provider of the magnetic properties is the inorganic part, whereas significant second-order NLO responses are more frequently originated from the organic

† Dipartimento di Chimica Inorganica, Metallorganica e Analitica, Università di Milano.
‡ Università dell'Insubria.
§ Dipartimento di Chimica Strutturale e Stereochimica Inorganica, Università di Milano.
|| Dipartimento di Chimica Università di Firenze.

(1) Knutson, J. L.; Martin, D. J.; Mitzi, D. B. *Inorg. Chem.* **2005**, *44*, 4699. Rabu, P.; Drillon, M. *Adv. Eng. Mat.* **2003**, *5*, 189. Coe, B. J.; Curati, N. R. *Comments Inorg. Chem.* **2004**, *25*, 147.
(2) See, for example: *Functional Hybris Materials*; Gomez-Romero, P., Sanchez, C., Eds.; Wiley-VCH Verlag GmbH & Co. KgaA: Weinheim, Germany, 2004.
(3) (a) Lacroix, P. G. *Chem. Mater.* **2001**, *13*, 3495. (b) Coronado, E.; Galán-Mascarós, J. R.; Romero, F. In *Functional Hybris Materials*; Gomez-Romero, P., Sanchez, C., Eds.; Wiley-VCH Verlag GmbH & Co. KgaA: Weinheim, Germany, 2004.

10.1021/ja0710712 CCC: $37.00

Scheme 1

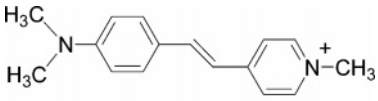

trans-4-(4-dimethylaminostyryl)-1-methylpyridinium

counterpart. For this purpose, the essential requirement is a large molecular first-order hyperpolarizability β of the chromophore, typically obtained in planar conjugated π-electron systems, end capped with electron-donor and -acceptor moieties.[4,5] According to the "two-level model",[6] β depends on the energy gap and the transition dipole moment between a polar ground state and a charge-separated first excited state.

In addition to the molecular properties, it is also essential that the supramolecular organization of the chromophores maximizes the bulk electro-optic response, first of all crystallizing in noncentrosymmetric space groups and then optimizing the phase matching.[7] In this respect, we must consider that even minor changes of the inorganic framework may affect the whole crystalline structure, inducing the NLO efficiency.

Recently, some of us have reported the synthesis as well as structural and photophysical characterization[8,9] of a new class of layered Cu(I) and Ag(I) inorganic−organic hybrids, involving self-organized organic cationic NLO-phores, characterized by an exceptional second-harmonic generation (SHG). However, samples of these materials are obtained only as microscopic crystals. In the search for highly active SHG hybrid materials obtainable as single crystals on a large scale, we investigated if the same kind of cationic second-order NLO-phores, in particular [DAMS$^+$] (*trans*-4-(4-dimethylaminostyryl)-1-methylpyridinium) (Scheme 1), can be self-organized within a different inorganic framework to generate a large SHG.

Some layered polymeric mixed M(II)/M(III) metal oxalates have been recently reported as convenient structural frameworks to produce interesting second-order NLO hybrid materials involving [DAMS$^+$] or [DAMS$^+$]-type cations.[10] However, because a noncentrosymmetric crystalline framework is not always guaranteed for this class of materials, we considered it relevant to extend the investigation to chiral M(III) oxalates, initially of Rh(III), since the Cr(III) and Fe(III) oxalates easily undergo racemization. We were in the meantime particularly concerned with connecting second-order NLO and magnetic properties in chiral materials, a field currently under deep investigation.[11] The initial study was thus mainly intended as a preliminary step in order to define the experimental conditions necessary to obtain stable chiral layered mixed metal oxalates. Therefore, we first assembled racemic Rh(III) oxalates with Mn(II) and [DAMS$^+$] under different reaction conditions in order to find the best experimental procedure to obtain, also with the Rh(III) ion, the same layered mixed M(II)/M(III) metal oxalates described in the literature.[10] During this study, we isolated a crystalline material which showed exceptional SHG and was characterized by a different and yet unobserved layered crystalline framework, corresponding to $[DAMS]_4[Rh_2Mn(C_2O_4)_6]\cdot 2DAMBA\cdot 2H_2O$ (**1**) (DAMBA = *p*-N(CH$_3$)$_2$C$_6$H$_4$CHO).

Scheme 2

$[DAMS]_4[Rh_2Mn(C_2O_4)_6]\cdot 2DAMBA\cdot 2H_2O$	**1**
$[DAMS]_4[Fe_2Mn(C_2O_4)_6]\cdot 2DAMBA\cdot 2H_2O$	**2**
$[DAMS]_4[Cr_2Mn(C_2O_4)_6]\cdot 2DAMBA\cdot 2H_2O$	**3**
$[DAMS]_4[Rh_2Zn(C_2O_4)_6]\cdot 2DAMBA\cdot 2H_2O$	**4**
$[DAMS]_4[Fe_2Zn(C_2O_4)_6]\cdot 2DAMBA\cdot 2H_2O$	**5**
$[DAMS]_4[Cr_2Zn(C_2O_4)_6]\cdot 2DAMBA\cdot 2H_2O$	**6**

This finding prompted us to investigate in depth a synthetic strategy for this new class of hybrid mixed metal oxalates, and eventually we have been able to identify a new promising family (see Scheme 2) of magnetic and NLO hybrid materials, which can be easily obtained as single crystals. The insertion of various magnetic (Cr(III), Fe(III), Mn(II)) and diamagnetic (Rh(III), Zn(II)) metal ions within the new structural motif allowed also an investigation of the tunability of the magnetic properties of these materials, still maintaining the very high SHG efficiency.

Experimental Section

General Comments. $K_3[M(C_2O_4)_3]\cdot nH_2O$ (M = Rh, Cr,[12] and Fe[13]) were prepared according to the literature. [DAMS]I, $Mn(NO_3)_2\cdot nH_2O$, and $ZnSO_4\cdot 7H_2O$ were purchased from Sigma-Aldrich and used without further purification. All compounds were characterized by XRPD, XRD (when single crystals suitable for diffraction studies were obtained). Elemental analyses (C, H, N) were carried out in the Dipartimento di Chimica Inorganica, Metallorganica e Analitica of the University of Milano, while O, M(II), M(III) analyses were carried out by Redox Lab, Milano. UV−vis spectra were recorded on a Jasco V-530 spectrophotometer.

Preparation of Phase α_{Rh}, α_{Fe}, α_{Cr}. In a 100 mL two-necked flask [DAMS]I (183.2 mg, 0.50 mmol) was dissolved in 40 mL of H_2O/CH_3OH (1/1), the solution was heated at 60 °C, and $K_3[M(C_2O_4)_3]\cdot nH_2O$ (M = Rh, Fe, Cr) (0.50 mmol) dissolved in 20 mL of H_2O/CH_3OH (1/1) was added. The heating was turned off, and $Mn(NO_3)_2\cdot nH_2O$ (147.8 mg, 0.50 mmol) dissolved in CH_3OH (2−3 mL) was added

(4) (a) Verbiest, T.; Houbrechts, S.; Kauranen, M.; Clays, K.; Persoons, A. *J. Mater. Chem.* **1997**, *7*, 2175. (b) Dalton, L. R.; Steier, W. H.; Robinson, B. H.; Zhang, C.; Ren, A.; Garner, S.; Chen, A.; Londergan, T.; Irwin, L.; Carlson, B.; Fifield, L.; Phelan, G.; Kincaid, C.; Amend, J.; Jen, A. *J. Mater. Chem.* **1999**, *9*, 1905. (c) Molecular Nonlinear Optics: Materials, Phenomena and Devices (Zyss, J., Ed.). *Chem. Phys.* **1999**, *245*.

(5) (a) Meredith, G. R. In *Non-Linear Optical Properties of Organic and Polymeric Materials*; Williams, J. D., Ed.; ACS Symposium Series; American Chemical Society: Washington, DC, 1983; pp 27−56. (b) Nonlinear Optical Properties of Organic Molecules and Crystals; Chemla, D. S., Zyss, J., Eds.; Academic Press: Orlando, FL, 1987; Vol. 1. (c) *Materials for Nonlinear Optics Chemical Perspectives*; Marder, S. R., Stucky, G. D., Sohn, J. E., Eds.; ACS Symposium Series 455; American Chemical Society: Washington, DC, 1991. (d) *Introduction to Nonlinear Optical Effects in Molecules and Polymers*; Prasad, P. N., Williams, D. J., Eds.; John Wiley: New York, 1991. (e) *Molecular Nonlinear Optics: Materials, Physics and Devices*; Zyss, J., Ed.; Academic Press: New York, 1994. (f) *Organic Nonlinear Optical Materials*; Bosshard, C., Sutter, K., Prêtre, P., Hulliger, J., Flörsheimer, M., Kaatz, P., Günter, P., Eds.; Advances in Nonlinear Optics; Gordon & Breach: Amsterdam, 1995; Vol. 1. (g) *Nonlinear Optics of Organic Molecules and Polymers*; Nalwa, H. S., Miyata, S., Eds.; CRC Press: Boca Raton, FL, 1997.

(6) (a) Oudar, J. L.; Chemla, D. S. *J. Chem. Phys.* **1977**, *66*, 446. (b) Oudar, J. L. *J. Chem. Phys.* **1977**, *67*, 2664.

(7) (a) Zyss, J.; Oudar, J. L. *Phys. Rev. A* **1982**, *26*, 2028. (b) Zyss, J.; Chemla, D. S. In *Nonlinear Optical Properties of Organic Molecules and Crystals*; Chemla, D. S. J., Zyss, J., Eds; Academic Press Inc.: Orlando, FL, 1987; Vol. 1, pp 23−187.

(8) Cariati, E.; Ugo, R.; Cariati, F.; Roberto, D.; Masciocchi, N.; Galli, S.; Sironi, A. *Adv. Mater.* **2001**, *13*, 1665.

(9) Cariati, E.; Macchi, R.; Roberto, D.; Ugo, R.; Galli, S.; Masciocchi, N.; Sironi, A. *Chem. Mater.*, in press.

(10) (a) Bénard, S.; Yu, P.; Coradin, T.; Rivière, E.; Clément, R. *Adv. Mater.* **1997**, *9*, 12. (b) Bénard, S.; Yu, P.; Audière, P.; Rivière, E.; Clément, R.; Guilhem, J.; Tchertanov, L.; Nakatami, K. *J. Am. Chem. Soc.* **2000**, *122*, 9444. (c) Evans, J.S.O.; Bénard, S.; Yu, P.; Clément, R. *Chem. Mater.* **2001**, *13*, 3813.

(11) See, for example: (a) Inoue, K.; Kikuchi, K.; Ohba, M.; Okawa, H. *Angew. Chem., Int. Ed.* **2003**, *42*, 4810. (b) Waniere, G.; Mejer, A. *Chem. Phys. Lett.* **1984**, *110*, 546. (c) Rikken, G. L. J. A.; Raupach, E. *Nature* **1997**, *390*, 493.

(12) Werner, A.; Poupardin, J. *Ber.* **1914**, *47*, 1955.

(13) Bailar, J. C.; Jones, E. M. *Inorg. Synth.* **1939**, *1*, 35.

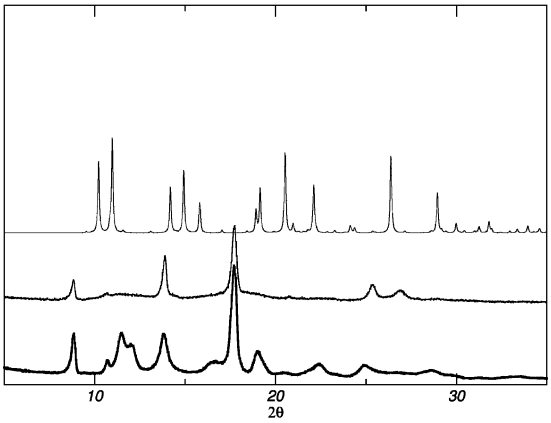

Figure 1. XRP diffractograms of two different phases α_{Rh} (lower and central diagrams), isolated using slightly different synthetic procedures and the simulated XRP diffractogram of the layered mixed metal oxalate [DAMS][$MnCr(C_2O_4)_3$] according to Clément et al. (upper diagram).[10c]

to the still hot solution. A brownish-black precipitate, α_{Rh}, α_{Fe}, or α_{Cr}, separated immediately. After 1.5 h of stirring at room temperature, the solid was filtered, washed with few drops of H_2O/CH_3OH (1/1), and dried under vacuum. It was characterized by a large SHG (same order of magnitude of [DAMS][*p*-toluenesulfonate])[14] working with an incident wavelength of 1907 nm.

Anal. Found α_{Rh}: (interval refers to a series of different preparations) C%, 45.63−44.21; H%, 4.64−3.99; N%, 5.93−4.01; O%, 23.97 (O% could be underestimated due to the formation of metal oxides during combustion); Mn%, 6.53; Rh% 10.92.

Anal. Found α_{Fe}: (interval refers to a series of different preparations) C%, 46.00−47.09; H%, 3.77−3.98; N%, 5.36−6.73; O%, 26.75 (O% could be underestimated due to the formation of metal oxides during combustion), Mn%, 7.25; Fe%, 4.98.

Anal. Found α_{Cr}: (interval refers to a series of different preparations) C%, 46.29−47.86; H%, 3.88−4.75; N%, 5.42−6.03; O%, 23.39 (O% could be underestimated due to the formation of metal oxides during combustion); Mn%, 7.68−8.21; Cr%, 4.60−5.35.

Attempts to grow suitable single crystals for X-ray diffraction from dissolution in hot H_2O followed by slow cooling at room temperature and then 0 °C failed. In the case of α_{Rh} and α_{Cr} the formation of centric [DAMS]$_5$[$Rh(C_2O_4)_3$]$I_2\cdot 6H_2O$ and [DAMS]$_5$[$Cr(C_2O_4)_3$]$I_2\cdot 6H_2O$, as revealed by single-crystal X-ray diffraction,[15] was observed.

Surprisingly, when $K_3[Rh(C_2O_4)_3]\cdot 4.5H_2O$ recrystallized from H_2O/MeOH is used as starting material, the reaction is reproducibly directed toward the formation of a phase α_{Rh} characterized by a slightly different XRPD (Figure 1) which shows an SHG of the same order of magnitude of [DAMS][*p*-toluenesulfonate][14] working with an incident wavelength of 1907 nm. Anal. Found: C% 44.99; H%, 4.22; N%, 5.36; O%, 25.73 (could be underestimated due to the formation of metal oxides during combustion); Mn%, 4.47; Rh%, 12.42

By leaving the filtrate obtained after separation of phase α_{Rh} (or α_{Cr}) under stirring at room temperature overnight, a new brownish-red precipitate, phase β_{Rh} (or β_{Cr}), characterized by an XRPD pattern slightly different from that of α_{Rh} (or α_{Cr}), was obtained. The solid was filtered, washed with H_2O/CH_3OH (1/1), and dried under vacuum. This solid was characterized by a rather low SHG (about 4 times the standard urea) working with an incident wavelength of 1907 nm.

Anal. Found β_{Rh}: C%, 48.42; H%, 4.97; N%, 6.98. Single crystals suitable for X-ray diffraction analysis could not be obtained.

Anal. Found β_{Cr}: C%, 50.65; H%, 5.24; N%, 7.31. Single crystals suitable for X-ray diffraction analysis could not be obtained.

From the reaction mother liquor after the separation of α_{Rh} and β_{Rh} we obtained, after 6 months, a very small amount of well-grown single crystals, suitable for X-ray diffraction characterization, of [$Rh_2Mn(C_2O_4)_6$][DAMS]$_4\cdot$2DAMBA$\cdot 2H_2O$ (**1**).

After filtration of phases α_{Cr} and β_{Cr}, a small amount of centrosymmetric [DAMS]$_5$[$Cr(C_2O_4)_3$]$I_2\cdot 6H_2O$, as revealed by X-ray single-crystal diffraction,[15] separated from the mother liquor after 3 weeks.

Preparation of Phase α^*_{Rh}, α^*_{Fe}, α^*_{Cr} . In a 100 mL two-necked flask [DAMS]I (183.0 mg, 0.50 mmol) was dissolved in 40 mL of H_2O/CH_3OH (1/1), the solution was heated at 60 °C, and $K_3[M(C_2O_4)_3]\cdot nH_2O$ (M = Rh, Fe, Cr) (0.50 mmol) dissolved in 20 mL of H_2O/CH_3OH (1/1) was added. The heating was turned off, and $ZnSO_4\cdot 7H_2O$ (146.3 mg, 0.50 mmol) dissolved in CH_3OH (2−3 mL) was added to the still hot solution. A brownish-black precipitate, α^*_{Rh}, α^*_{Fe}, or α^*_{Cr}, separated immediately. After 1.5 h of stirring at room temperature, the solid was filtered, washed with a few drops of H_2O/CH_3OH (1/1), and dried under vacuum. It was characterized by a large SHG (same order of magnitude of [DAMS][*p*-toluenesulfonate])[14] working with an incident wavelength of 1907 nm.

Anal. Calcd α^*_{Rh}: Found (interval refers to a series of different preparations) C%, 40.73−42.24; H%, 3.15−3.25; N%, 5.01−4.65; O%, 25.84 (O% could be underestimated due to the formation of metal oxides during combustion); Zn%, 8.24; Rh%, 13.67.

Anal. Calcd α^*_{Fe}: Found (interval refers to a series of different preparations) C%, 44.42−43.80; H%, 3.77−3.61; N%, 5.40−4.93; O%, 26.77 (O% could be underestimated due to the formation of metal oxides during combustion); Zn%, 8.02; Fe%, 4.88.

Anal. Calcd α^*_{Cr}: Found (interval refers to a series of different preparations) C%, 42.35−43.10; H%, 3.22−3.34; N%, 4.23−5.05; O%, 27.66 (O% could be underestimated due to the formation of metal oxides during combustion); Zn%, 7.65; Cr%, 7.11.

Attempts to grow suitable single crystals for X-ray diffraction analysis by dissolution in hot H_2O/MeOH (1:1), followed by slow cooling at room temperature and then at 0 °C, failed due to the formation of powders of crystallinity not sufficient for X-ray identification.

Synthesis of 1−6. In a 100 mL flask DAMBA (20.5 mg; 0.14 mmol) was added to the corresponding phase α or α^* (80.0 mg), prepared as above-reported, dissolved in 70 mL of H_2O. The solution was heated under reflux for 1.5 h and then cooled at room temperature. On standing overnight, the formation of a greenish compound with a metallic luster was observed. After filtration, the compound was dried under vacuum.

Anal. Calcd for $C_{94}H_{102}MnN_{10}O_{28}Rh_2$ (**1**): C%, 54.26; H%, 4.94; N%, 6.73. Found: C%, 53.96; H%, 5.10; N%, 6.67.

Anal. Calcd for $C_{94}H_{102}Fe_2MnN_{10}O_{28}$ (**2**): C%, 56.83; H%, 5.80; N%, 7.05. Found: C%, 56.68; H%, 5.60; N%, 7.03.

Anal. Calcd for $C_{94}H_{102}Cr_2MnN_{10}O_{28}$ (**3**): C%, 57.06; H%, 5.20; N%, 7.08. Found: C%, 56.94; H%, 5.23; N%, 7.09.

Anal. Calcd for $C_{94}H_{102}N_{10}O_{28}Rh_2Zn$ (**4**): C%, 53.99; H%, 4.92; N%, 6.70. Found: C%, 54.16; H%, 5.02; N%, 6.55.

Anal. Calcd for $C_{94}H_{102}N_{10}O_{28}Fe_2Zn$ (**5**): C%, 56.54; H%, 5.15; N%, 7.01. Found: C%, 56.44; H%, 5.03; N%, 7.05.

Anal. Calcd for $C_{94}H_{102}N_{10}O_{28}Cr_2Zn$ (**6**): C%, 56.76; H%, 5.17; N%, 7.04. Found: C%, 56.56; H%, 5.06; N%, 6.98.

Solid-State SHG by Kurtz−Perry Measurements. The 1064 nm initial wavelength of a Nd:YAG pulsed laser beam was shifted to 1907 nm by stimulated scattering in a high-pressure hydrogen cell. A portion of this beam was directed on capillaries containing the samples. The scattered radiation was collected by an elliptical mirror, filtered in order to select only the second-order contribution, and recollected with a Hamamatsu R5108 photomultiplier tube. SHG efficiency was evaluated by taking as a reference the SHG signal of [DAMS][*p*-toluenesulfonate][14] or urea.

(14) Marder, S. R.; Perry, J. W.; Yakymyshyn, C. P. *Chem. Mater.* **1994**, *6*, 1137.

(15) Cell dimensions: $a = 14.352(1)$ Å; $b = 15.395(1)$ Å; $c = 20.771(1)$ Å; $\alpha = 100.903(2)°$, $\beta = 96.813(2)°$; $\gamma = 100.466(2)°$. An isomorphous structure containing Rh(II) was solved from single-crystal X-ray analysis, and it is reported in the crystallographic Supporting Information (compound **10**).

Table 1. Crystal Data and Structure Refinement for Compounds **1**−**3** $[DAMS]_4[M(III)_2Mn(C_2O_4)_6]\cdot 2DAMBA\cdot 2H_2O$ (M = Rh, Fe, Cr)[a]

compd empirical formula	$C_{94}H_{102}MnN_{10}O_{28}Rh_2$	$C_{94}H_{102}Fe_2MnN_{10}O_{28}$	$C_{94}H_{102}Cr_2MnN_{10}O_{28}$
formula weight	2080.62	1986.50	1978.80
temperature	150(2) K	293(2) K	293(2) K
wavelength	0.710 73 Å	0.710 73 Å	0.710 73 Å
crystal system, space group	orthorhombic, *Fdd*2	orthorhombic, *Fdd*2	orthorhombic, *Fdd*2
unit cell dimensions	$a = 38.937(3)$ Å	$a = 39.406(3)$ Å	$a = 39.299(2)$ Å
	$b = 48.000(4)$ Å	$a = 48.573(4)$ Å	$b = 48.612(3)$ Å
	$c = 9.5196(7)$ Å	$c = 9.4673(8)$ Å	$c = 9.4962(6)$ Å
volume	17 792(4) Å^3	18 121.7(19) Å^3	18 141.7(19) Å^3
Z, calcd density	8, 1.553 Mg/m^3	8, 1.456 Mg/m^3	8, 1.449 Mg/m^3
absorption coefficient	0.596 mm^{-1}	0.541 mm^{-1}	0.460 mm^{-1}
F(000)	8600	8296	8264
crystal size	0.15 × 0.02 × 0.02 mm^3	0.3 × 0.2 × 0.15 mm^3	0.2 × 0.05 × 0.05 mm^3
θ range for data collection	1.35° to 25.02°	1.33° to 27.51°	1.33° to 28.12°
reflections collected/unique	36 668/7844	45 494/7437	43 574/9979
R(int)	0.071	0.049	0.134
R_σ	0.057	0.045	0.196
max and min transmission	1.0 and 0.883	1.0 and 0.886	1.0 and 0.842
data/restraints/parameters	7844/1/609	7437/1/609	9979/1/609
goodness-of-fit on F^2	1.066	1.046	0.969
final *R* indices [$I > 2\sigma(I)$]	$R_1 = 0.0468$, $wR_2 = 0.1106$	$R_1 = 0.0507$, $wR_2 = 0.1213$	$R_1 = 0.0864$, $wR_2 = 0.2069$
R indices (all data)	$R_1 = 0.0703$, $wR_2 = 0.1274$	$R_1 = 0.0849$, $wR_2 = 0.1443$	$R_1 = 0.2281$, $wR_2 = 0.2838$
largest diff peak and hole	1.108 and −1.263 e·A^{-3}	0.737 and −0.660 e·A^{-3}	0.792 and −0.813 e·A^{-3}

[a] $R_{int} = \Sigma|F_o^2 - F_{mean}^2|/\Sigma F_o^2$; $R_\sigma = \Sigma\sigma(F_o^2)/\Sigma F_o^2$; $R_1 = \Sigma||F_o| - |F_c||/\Sigma|F_o|$; $wR_2 = (\Sigma(F_o^2 - F_c^2)^2/\Sigma wF_o^4)^{1/2}$.

Magnetic Measurements. The measurements were performed by using a Cryogenic S600 SQUID magnetometer operating between 2 and 300 K and with an applied field ranging from 0 to 6 T. All the samples were prepared by grinding freshly filtered crystals and then wrapping the powder in Teflon tape. Magnetic susceptibilities were corrected for diamagnetism by using Pascal's constants. The diamagnetic contributions of the sample holder and the Teflon tape were independently measured and subtracted.

Details of the fitting of the experimental data and of the Curie−Weiss low plots are reported in the Supporting Information.

X-ray Single-Crystal Diffraction. Crystals suitable for X-ray diffraction of compounds **1**, **2**, and **3** were obtained by leaving the reaction solution for a few days at room temperature.

Crystals were mounted on a glass fiber and collected on a Bruker SMART CCD (**1** and **2**) and a Bruker SMART-APEX CCD area-detector diffractometer (**3**). **1** was collected under a nitrogen stream at 150 K while the other species were analyzed in air at room temperature. Crystal data are reported in Table 1.

Graphite-monochromatized Mo Kα ($\lambda = 0.710\ 73$ Å) radiation was used with the generator working at 45 kV and 40 mA (SMART) or 50 kV and 30 mA (SMART-APEX). Orientation matrixes were initially obtained from least-squares refinement on ca. 300 reflections measured in three different ω regions, in the range $0 < \theta < 23°$; cell parameters were optimized on the position, determined after integration, of all reflections above the 10 $\sigma(I)$ level. For **1**, **2**, and **3**, 1800 frames, at 80, 30, and 40 s per frame, respectively, were collected with $\Delta\omega = 0.3°$ and intensities within the limits $0 < 2\theta < 50°/55°/56°$, respectively, in the full sphere (ω scan method). Sample−detector distances were set at 3.8 (SMART) and 4.7 cm (SMART-APEX); an empirical absorption correction was applied (SADABS).[16]

The first structure was solved by direct methods (using SIR97,[17] within the WINGX[18] suite of programs), and on this solution all structures were subsequently refined with full-matrix least-squares (SHELX97)[19] on F^2 on the basis of the independent reflections reported in Table 1; anisotropic temperature factors were assigned to all non-hydrogenic atoms. Hydrogens were riding on their carbon atoms, though water hydrogens were not located and included in our solutions. Results of the refinements are also reported in Table 1.

X-ray Powder Diffraction Analysis. The powders of all phases α and β analyzed were gently ground in an agate mortar and then cautiously deposited in the hollow of an aluminum holder equipped with a zero background plate with the aid of a glass slide. Diffraction data (Cu Kα, $\lambda = 1.5418$ Å) were collected on a vertical scan Philips PW1820 diffractometer with the generator operating at 40 kV and 40 mA. Intensities were measured in the range $5° < 2\theta < 35°$, typically with step scans of 0.02° (10 s/step).

Results and Discussion

The most common classes of hybrid inorganic−organic materials with very large second-order NLO properties are those where the inorganic and organic components are clearly segregated. Examples are the layered materials of Cu(I) or Ag(I) corresponding to the stoichiometry $[DAMS][M_5I_6]$[8] or the intercalated materials obtained by ionic exchange of $[DAMS^+]$ into the layered structure of MPS_3 (M = Mn, Zn, Cd).[20] In all these compounds the very large SHG is originated by a specific order of the $[DAMS^+]$ NLO-phore between the inorganic layers, which stabilize a J-aggregate kind[21] of arrangement of the NLO-phore.

In this field certainly fall the layered mixed M(II)/M(III) metal oxalates involving $[DAMS^+]$ and a series of $[DAMS^+]$-type cations described by Clément and co-workers, who first devised, for this class of hybrid materials, the coupling of magnetic and second-order NLO properties,[10] generating therefore new multiproperty materials.

As stated in the introduction, we tried to synthesize Clément's layered mixed M(II)/M(III) metal oxalates of $[DAMS^+]$, with M(III) metal ions such as Rh(III), whose oxalates are sufficiently stable against racemization,[22] thus ensuring the acentricity of

(16) Sheldrick, G. M. *SADABS 2004/1*; University of Göttingen: Germany, 2004.
(17) Altomare, A.; Burla, M. C.; Camalli, M.; Cascarano, G. L.; Giacovazzo, C.; Guagliardi, A.; Moliterni, A. G. G.; Polidori, G.; Spagna, R. *J. Appl. Crystallogr.* **1999**, *32*, 115−119.
(18) Farrugia, L. J. *J. Appl. Crystallogr.* **1999**, *32*, 837−838.
(19) Sheldrick, G. M. *SHELX97-Program for the refinement of Crystal Structure*; University of Göttingen: Germany, 1997.
(20) Lacroix, P. G.; Veret Lemarinier, A. V.; Clemènt, R.; Nakatani, K.; Delaire, J. A. *J. Mater. Chem.* **1993**, *3*, 499. Lacroix, P. G.; Clemènt, R.; Nakatani, K.; Delaire, J. A.; Zyss, J.; Ledoux, I. *Science* **1994**, *263*, 658. Corradin, T.; Clemènt, R.; Lacroix, P. G.; Nakatani, K. *Chem. Mater.* **1996**, *8*, 2153.
(21) Mobius, D. *Adv. Mater.* **1995**, *7*, 437.

the crystalline framework, a prerequisite for SHG. In order to identify the synthetic method to obtain Rh(III)-based layered mixed oxalates with the cation [DAMS$^+$] and Mn(II), we first used racemic Rh(III) oxalate. Each reaction product was typically scrutinized by the Kurtz−Perry method[23] and X-ray powder diffraction (XRPD). In fact the structures identified by Clément and co-workers, by an *ab initio* X-ray powder investigation,[10c] show a well characterized XRPD pattern controlled by the inorganic layers (see Figure 1).

Synthesis, Characterization, and Optical Properties. When mixing in water $K_3[Rh(C_2O_4)_3]\cdot 4.5H_2O$, $Mn(NO_3)_2$ and [DAMS]I (reaction 1; see Experimental Section), we observed the separation of a partially crystalline phase, $\boldsymbol{\alpha_{Rh}}$, characterized by a very large SHG of the same order of magnitude as that of [DAMS][*p*-toluenesulfonate][14] working at a 1907 nm nonresonant incident wavelength:

$$K_3[Rh(C_2O_4)_3]\cdot 4.5H_2O + Mn(NO_3)_2 + [DAMS]I \xrightarrow[1.5\ h]{H_2O/MeOH\ (1/1)} \boldsymbol{\alpha_{Rh}} \quad (1)$$

After 24 h a minor amount of a far less NLO active phase $\boldsymbol{\beta_{Rh}}$ (SHG 4 times that of urea at 1907 nm) separated from the mother liquor. The XRPD patterns of both phases were not retraceable to that expected for a [DAMS$^+$] metal oxalate described by Clément et al.[10c]

Unfortunately, we were unable to obtain suitable single crystals from the recrystallization of either phases, and at the same time, any attempt to determine the crystalline metrics together with a tentative structural definition from *ab initio* powder diffraction analyses failed. Also the analytical data of both $\boldsymbol{\alpha_{Rh}}$ and $\boldsymbol{\beta_{Rh}}$ phases obtained in a series of reactions were quite different from those expected for a Clément's like material[10] and not satisfactory for the definition of a reproducible stoichiometry for any of them (see the Experimental Section). From atomic absorption analysis we could just assess the presence of both metals with variable Rh(III)/Mn(II) ratios (ranging from 0.89 to 1.48). Different synthetic procedures for $\boldsymbol{\alpha_{Rh}}$ always afforded microcrystalline phases characterized by a very large SHG but somewhat different analytical data and diffractograms, with subsets of common peaks together with slightly variable (even disappearing) ones (see Figure 1). Therefore $\boldsymbol{\alpha_{Rh}}$ actually appears to be a mixture of phases of low crystallinity, whose composition is strongly dependent on reaction conditions.

Finally, from the reaction mother liquor, after the separation of $\boldsymbol{\alpha_{Rh}}$ and $\boldsymbol{\beta_{Rh}}$, we obtained, after several weeks, a very small amount of well-grown single crystals, suitable for X-ray diffraction characterization, corresponding to a new crystalline phase of formula $[DAMS]_4[Rh_2Mn(C_2O_4)_6]\cdot 2DAMBA\cdot 2H_2O$ (**1**). By the Kurtz−Perry method, working with a nonresonant wavelength of 1907 nm, **1** showed an extremely high SHG (same order of magnitude as that of [DAMS][*p*-toluenesulfonate] at the same wavelength).[14] The basic stoichiometry of **1** was somewhat surprising due to the unexpected presence of DAMBA, probably originated by a slow Rh(III) catalyzed oxidation of the ethylenic bond of [DAMS$^+$], being the starting [DAMS]I used in the synthesis a pure compound, as evidenced by ^{1}H NMR spectroscopy.

After the serendipitous isolation of **1**, we investigated the best reaction conditions to obtain it in large amounts by mixing the reagents of reaction 1 directly with the required stoichiometric amount of DAMBA. However this method never produced pure **1** but always multiphase mixtures. We obtained **1** in high yields only by adding DAMBA directly to a phase $\boldsymbol{\alpha_{Rh}}$ dissolved in H_2O (reaction 2; see the Experimental Section).

$$\boldsymbol{\alpha_{Rh}} + DAMBA \xrightarrow[reflux,\ 1.5\ h]{H_2O} [DAMS]_4[Rh_2Mn(C_2O_4)_6]\cdot 2DAMBA\cdot 2H_2O \quad (2)$$

The combination of reactions 1 and 2 proved to be a general high yield method for the synthesis of a new class of hybrid materials isostructural to **1** by varying M(III) (using for example Cr or Fe instead of Rh) or M(II) (using Zn instead of Mn). Therefore, we successfully applied reaction 1 to Cr(III) and Fe(III) oxalates to produce the microcrystalline phases $\boldsymbol{\alpha_{Cr}}$ or $\boldsymbol{\alpha_{Fe}}$ with XRPD patterns and SHGs similar to those of $\boldsymbol{\alpha_{Rh}}$. Despite a slightly higher degree of crystallinity with respect to $\boldsymbol{\alpha_{Rh}}$, single crystals suitable for X-ray diffraction analysis could not be obtained even for $\boldsymbol{\alpha_{Cr}}$ and $\boldsymbol{\alpha_{Fe}}$. These were then used as starting materials to obtain, following reaction 2, single crystals of $[DAMS]_4[Fe_2Mn(C_2O_4)_6]\cdot 2DAMBA\cdot 2H_2O$ (**2**) and $[DAMS]_4[Cr_2Mn(C_2O_4)_6]\cdot 2DAMBA\cdot 2H_2O$ (**3**). Like the isostructural material based on Rh(III) (**1**), both **2** and **3** show an SHG, at 1907 nm, of the same order of magnitude as that of [DAMS][*p*-toluenesulfonate] (about 1000 times that of urea).[14] The isolation of $\boldsymbol{\alpha_{Cr}}$ is unexpected since, under rather similar reaction conditions, formation of the layered mixed metal oxalate $[DAMS][MnCr(C_2O_4)_3]$, characterized by a quite different XRPD diffraction pattern, is known to take place.[10c]

After 24 h, as in the case of Rh(III), a second microcrystalline phase $\boldsymbol{\beta_{Cr}}$ separated.[24] Its SHG (4 times that of urea at a 1907 nm incident wavelength), XRPD diffraction pattern, and elemental analysis (see the experimental part) were not consistent with those expected for the layered mixed metal oxalate $[DAMS][MnCr(C_2O_4)_3]$.[10b,c] It is worth mentioning that after separation of $\boldsymbol{\alpha_{Cr}}$ and $\boldsymbol{\beta_{Cr}}$ minor amounts of the centrosymmetric species $[DAMS]_5[Cr(C_2O_4)_3]I_2\cdot 6H_2O$[15] separated from the mother liquor within a few weeks. Interestingly, under the same reaction conditions, working with Rh(III) instead of Cr(III), **1** was obtained, confirming the fundamental role of Rh(III) in the partial oxidation of [DAMS$^+$] to DAMBA.

Any attempt to recrystallize the $\boldsymbol{\alpha_{Cr}}$ phase ended up in small amounts of NLO inactive crystalline materials such as $[DAMS]_5[Cr(C_2O_4)_3]I_2\cdot 6H_2O$,[15] always containing just the Cr(III) metal ion.

Once established the best synthetic procedure of this new class of hybrid materials, we exploited the design possibilities of the synthetic method, by changing the M(II) ion in order to differentiate the magnetic properties and to check if such a change could modify the SHG. Therefore, we reproduced reaction 1 with the substitution of the high spin $3d^5$ Mn(II) ion with the diamagnetic $3d^{10}$ Zn(II) ion. We thereby obtained the microcrystalline phases $\boldsymbol{\alpha^*_{Rh}}$, $\boldsymbol{\alpha^*_{Cr}}$, $\boldsymbol{\alpha^*_{Fe}}$, characterized by slightly higher crystallinity with respect to the corresponding ones containing Mn(II). However, even for these phases we were unable to obtain crystals suitable for X-ray structural determi-

(22) Vaughn, J. W.; Magnuson, V. E.; Seiler, G. J. *Inorg. Chem.* **1969**, *8*, 1201.
(23) Kurtz, S. K.; Perry, T. T. *J. Appl. Phys.* **1968**, *39*, 3798.
(24) At variance from Rh and Cr derivatives, no separation of $\boldsymbol{\beta_{Fe}}$ was observed from the mother liquor when the M(III) ion is Fe(III).

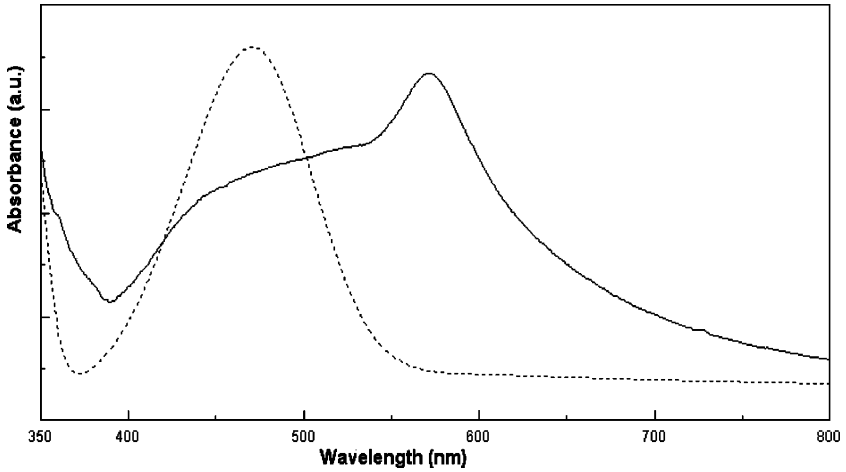

Figure 2. UV−vis spectra of **1**: in nujol (—) and CH_3CN (···).

nation. XRPD and the Kurtz−Perry test on α^*_{Rh}, α^*_{Cr}, α^*_{Fe} showed that substitution of Mn(II) with Zn(II) does not affect neither the diffraction pattern nor the SHG efficiency. By reaction 2 we thus obtained single crystals of $[DAMS]_4[Rh_2Zn(C_2O_4)_6]\cdot 2DAMBA\cdot 2H_2O$(**4**), $[DAMS]_4[Fe_2Zn(C_2O_4)_6]\cdot 2DAMBA\cdot 2H_2O$(**5**), and $[DAMS]_4[Cr_2Zn(C_2O_4)_6]\cdot 2DAMBA\cdot 2H_2O$ (**6**).

Interestingly, microcrystalline phases of the kind α_{Rh}, α_{Cr}, α_{Fe} cannot be obtained with all M(II) ions. For instance phases α^{**}_{Rh}, α^{**}_{Cr}, α^{**}_{Fe} were obtained with Ni(II) but not with Cu(II).

Surprising is the somewhat unique role of DAMBA in stabilizing the crystalline structure of **1**−**6**. In fact, by carrying reaction 2 in the presence of other *para* substituted benzaldehydes, we failed in producing crystalline compounds isomorphic to **1**−**6**. For example, [*p*-$CH(CH_3)_2C_6H_4CHO$] and [*p*-$(C_4H_9)_2NC_6H_4CHO$] gave one of the centrosymmetric materials containing only the M(III) ion and [$DAMS^+$] previously obtained in the attempted recrystallization of α_{Rh}, α_{Cr}, α_{Fe}, lacking both the aldehyde and the M(II) ion, while [*p*-$NO_2C_6H_4CHO$] gave a new crystalline phase with a different XRPD diffraction pattern not observed before but NLO inactive.

Solid-state UV−visible absorption spectra of **1**−**6** in nujol (the spectrum of **1** is reported as example in Figure 2), show the superposition of two bands: a broad and strong band centered around 464 nm and a strong, narrow signal at 568 nm, indicative of J aggregates of the [$DAMS^+$] cation.[8] When **1**−**6** are dissolved in acetonitrile, the absorption spectra are identical to that of [DAMS]I, with an absorption band at 471 nm (Figure 2) due to the disruption of the ordered J aggregates by dissolution in a polar organic solvent.

Structural Features of Compounds 1−6. The crystal structures of **1**−**6** are all isomorphous and belong to the polar acentric *Fdd*2 space group, as proven by single-crystal X-ray diffraction on **1**−**3** and XRPD on **4**−**6**. The large asymmetric unit contains two independent [$DAMS^+$] ions, one DAMBA, one water molecule, three oxalate anions, one M(III) ion lying in a general position, and one M(II) ion in a twofold special position (the only special position of this space group, occurring at (0,0,*z*)).

Differently from the other mixed M(II)/M(III) metal oxalates of [$DAMS^+$][10c] which are in keeping with the commonly observed honeycomb frameworks,[25] compounds **1**−**6** give rise to a new organic−inorganic 2D framework (rather than a purely inorganic one), controlling the segregation of layers of the [$DAMS^+$] NLO-phore, arranged as J aggregates,[21] whose macroscopic polarities result in being parallel as required to generate very large SHGs (see below).

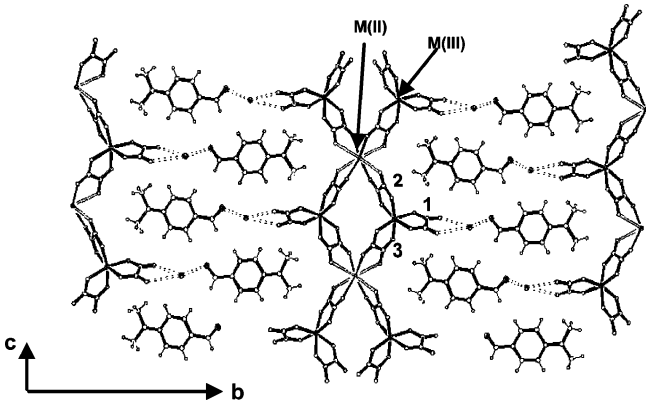

Figure 3. A view of the inorganic/organic layer characterizing **1**−**6** perpendicular to the crystallographic *a*-axis. M(II) and M(III) sites and independent oxalates 1, 2, and 3 are indicated, as well as the stronger hydrogen bonding connections, that involve the "lateral" oxalate ligands (having two free oxygens), the DAMBA molecules and the water molecules (whose hydrogens are not shown, because they were not included in structural refinement). Weaker C−H···O connections are not reported. The metal-oxalate stripes, elongated along the direction of the *c* crystallographic axis, can be recognized.

The inorganic part, composed by the two metal ions with coordinated oxalates, is characterized by infinite 1D "stripes" (∼14 Å large) (see Figure 3), elongated along the shorter *c*-axis and alternating a tilting of +15° and −15° with respect to the [1 0 0] plane. This arrangement produces the acentricity of the inorganic part, which would otherwise belong to the parent *Fddd* space group. The M(III) cation is side-on coordinated by three oxalate groups. One of them (oxalate 1) stretches out from the stripe, while the other two (bridging oxalates 2 and 3) interact with the M(II) cation. The latter site is bridged to four M(III) centers by four oxalate anions and can be regarded as tetra- or octacoordinated (within a strongly distorted tetragonal antiprism geometry). Four shorter (∼2.3 Å) and four longer (∼2.55 Å) M(II)−O distances are found, which slightly vary as a function of M(III) (see Table 2). It is relevant that the metal-oxalate

(25) Sometimes the honeycomb is distorted due to the extended coordination at M(II) as reported in Coronado, E.; Galan-Mascaros, J. R.; Martí-Gastaldo, C.; Martínez, M. *Dalton Trans.* **2006**, 3294.

Table 2. Long and Short Mn−O Distances in Compounds **1**−**3**[a]

	1	2	3
bridging oxalate 2	2.570(4) 2.356(4)	2.592(3) 2.265(3)	2.649(8) 2.322(8)
bridging oxalate 3	2.499(4) 2.382(4)	2.472(3) 2.295(3)	2.517(7) 2.348(8)

[a] Mn lies on a twofold axis; therefore there are only two independent oxalates (see Figure 3).

"stripe" is obtained from the combination of three- and tetraconnected M(III) and M(II) ions. 1D nets of this kind are quite rare, and only few examples are known in metal oxalates.[26] The octacoordination is not so unusual for the Mn(II) ion, especially when bound to chelating ligands, but only one example is known for polymeric oxalates.[27] On the other hand, the octacoordination is less common for the Zn(II) ion in inorganic complexes;[28] no example is known with oxalates.[29]

Note that, in order to obtain the 1D stripe, an antiprismatic octacoordination at M(II) is not strictly necessary and a distorted tetrahedral coordination would also be possible. The degree of asymmetry of the octacoordination could thus very likely vary with the nature and the size of M(II).

Each pair of stripes is spaced by ∼10 Å along *b* and shifted by one-half along *c*, producing a mismatch of the lateral branches (see Figure 3). The empty volume between the "stripes" is used to accommodate the DAMBA and the water molecules in a beautiful system acting as a bridge between the inorganic "stripes" to produce a compact mixed organic/inorganic layer overall parallel to [100], tightened by both coordinative bondings and hydrogen bonds (stronger O−H···O or weaker C−H···O; see Figure 3). In fact, the aldehydic group of DAMBA is connected by a hydrogen bond with a water molecule (dO···O ∼2.85 Å), which is also connected via hydrogen bond to the hemicoordinated lateral oxalate (dO···O ∼2.9 Å). The two methyl groups of the dimethylamino substituent form weaker hydrogen bonds with the oxalates of an adjacent "stripe". Thus, the role of DAMBA is not just that of filling the void in the 3D crystalline framework of **1**−**6** but actually of stabilizing, together with water molecules, the formation of a compact and flexible organic−inorganic layer.

The thickness of each organic/inorganic layer is ca. 3−4 Å (not very homogeneous, due to the mix of organic and inorganic parts), whereas the stratum of the organic NLO-phore [DAMS$^+$] is about 6−7 Å thick. This allows the aromatic rings of [DAMS$^+$] to arrange almost perfectly perpendicular with respect to the organic/inorganic layer (see Figure 4). Clément and co-workers[10b] noted an inverse correlation between the SHG activity and the separation of the two inorganic honeycomb layers in [organic-NLO-phore][MM′$(C_2O_4)_3$] mixed M(II)/M(III) metal oxalates crystallized in a monoclinic system (many NLO-phores or M/M′ pairs were scrutinized, and the interlayer separations were estimated on the basis of XRPD data). From the single-crystal determination reported for two similar, though centrosymmetric, compounds,[10b] it is possible to infer that the thickness of the honeycomb inorganic layer of the class of mixed

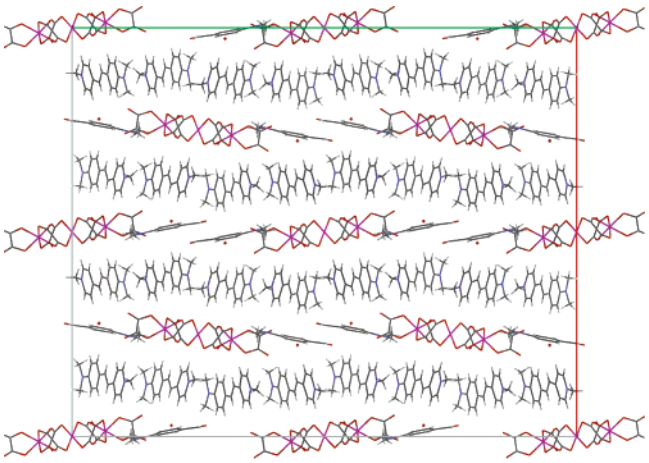

Figure 4. Wireframe plot showing the packing of anionic organic/inorganic and cationic organic layers in compounds **1**−**6** (viewed along *c*-axis). The unit cell box is drawn, while the hydrogen atoms are omitted for clarity.

M(II)/M(III) hybrid metal oxalates reported by Clément et al.[10] is about 3 Å and therefore the organic NLO-phore stratum in all examples reported in ref 10b should be about 5.5−6 Å thick. As suggested by Clément et al.,[10b,c] this very likely implies some tilting of the organic NLO-phore in [DAMS][MM′$(C_2O_4)_3$] with respect to a vector normal to the inorganic layer, a tilting which is instead almost negligible in compounds **1**−**6**. However, the very large SHG of **1**−**6** does not confirm the hypothesis that a shorter separation between the inorganic (or organic/inorganic) layers would favor a significant SHG.

The reasons beyond the different behavior in stabilizing different arrangements of the [DAMS$^+$] NLO-phore between [MM′$(C_2O_4)_3$] honeycomb layers and [MM′$(C_2O_4)_3$][DAMBA-$(H_2O)_2$] ones might stem from the different nature of the interaction with the NLO-phore. The former network is characterized by the periodic disposition of "octupolar" metals only, whereas the latter contains both "octupolar" and "quadrupolar" (or more precisely "hexadecapolar") metals; therefore in this latter case the charge distribution within the layer is less homogeneous due to the alternation of charged M$(C_2O_4)_3$ fragments and neutral DAMBA and H_2O spacers.

Inside the organic cationic layer, the [DAMS$^+$] NLO-phores are disposed parallel one to the other and head-to-tail arranged, alternating the two independent molecules of the asymmetric unit to form chains of cations that stack (spaced by ca. 3.45 Å) with about half a molecule mismatch typical of J aggregation[30] (see Figure 5) already suggested by the spectroscopic evidence (see Figure 2). All the chains within a given stratum have the same orientation while two adjacent strata alternate the chain directions, forming angles of +22° and −22° with respect to the polar axis c (see Figure 4). The formation of a full organic layer, instead of the piling of a single chain, allows hosting the push−pull [DAMS$^+$] NLO-phore with dipolar moment directions more properly oriented to generate a very large SHG as more thoroughly discussed in the next paragraph.

Structural Origin of the Superior SHG. According to the so-called "two-level model",[6] the *molecular* second-order NLO response of an organic NLO-phore can be ascribed to one major charge transfer (CT) process. In the *solid state*, however, the total SHG efficiency can be described as the sum of the

(26) (a) Armentano, D.; De Munno, G.; Mastropietro, T. F.; Julve, M.; Lloret, F. *Chem. Commun.* **2004**, 1160. (b) Rochon, F. D.; Melanson, R.; Andruh, M. *Inorg. Chem.* **1996**, *35*, 6086.
(27) Rochon, F. D.; Melanson, R.; Andruh, M. *Inorg. Chem.* **1996**, *35*, 6086.
(28) See for example Junk, P. C.; Smith, M. K.; Steed, J. W. *Polyhedron* **2001**, *20*, 2979.
(29) The Cambridge Structural Database, version 5.27, November 2005.
(30) Di Bella, S.; Ratner, M. A.; Marks, T. J. *J. Am. Chem. Soc.* **1992**, *114*, 5842.

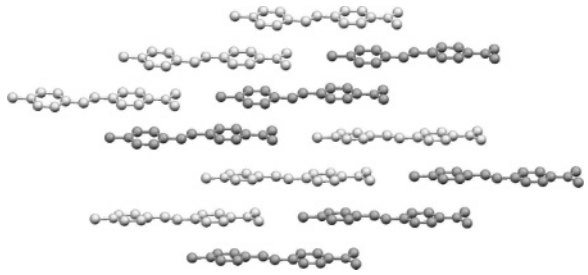

Figure 5. A view of one organic cationic layer formed by J type arrangement of [DAMS$^+$] molecules. The two independent [DAMS$^+$] molecules are shown in light and dark gray, respectively.

molecular contributions weighted for their orientation within the crystalline framework. This concept was successfully developed by Zyss,[7] who eventually proposed a set of geometrical relationships linking the molecular quadratic hyperpolarizability of the chromophore along the charge transfer axis (β_{CT}) to each element of the overall crystalline nonlinearity *per* molecule (b_{eff}). Thus, in order to identify the structural origin of the very large solid-state SHG of crystalline materials **1**−**6**, we evaluated the phase-matchable components of b_{eff} according to Zyss' geometrical model, starting from the crystalline structure above-reported and discussed.

In spite of the different metal centers, all materials **1**−**6** show comparable SHG efficiencies. It is thus very likely that any contribution to the SHG coming from the metal-to-ligand charge transfers should be almost negligible, compared to the strong SHG produced by a very efficient organic NLO-phore like [DAMS$^+$]. Such a statement is supported also by the highly symmetrical coordination spheres around the M(II) and M(III) metal centers, with three and four almost identical coordinating groups which do not favor significant contributions to the molecular second-order NLO response originated by dipolar terms of the coordination spheres.

Zyss' model was thus applied: (*i*) adopting an "oriented gas" model, i.e., supposing that all the [DAMS$^+$] chromophores interact only weakly;[31] (*ii*) assuming, at first approximation, that in all the materials **1**−**6** the SHG active chromophores can be described by a mono-dimensional system whose axis coincides with the CT direction; (*iii*) identifying the CT axis with the longest dipole moment inertial axis of the [DAMS$^+$] chromophore, i.e., with the N···N vector.

According to the *mm*2 crystallographic class of **1**−**6**, the independent phase-matchable components of b_{eff} are expressed as $b_{eff} = \sin^2(\phi)\cos(\theta)\sin^2(\theta)\beta_{CT}$ (for ZXX) and $b_{eff} = \cos^2(\phi)\cos(\theta)\sin^2(\theta)\beta_{CT}$ (for ZYY), where θ is the angle between the CT axis and the unique *c*-axis and ϕ is the angle between the *a*-axis and the projection of the CT axis on the *ab* plane. Given the orientation of the CT axis of the chromophores, ZXX is the only component that can significantly contribute to the SHG signal.[7] The optimum value of ZXX, $b_{eff}/\beta_{CT} = 0.385$, could be obtained for $\theta = 54.74°$.

In **1**−**6**, two crystallographically independent, but almost parallel, [DAMS$^+$] chromophores are present, with $|\theta|$ at about 22°, leading to $b_{eff}/\beta_{CT} = 0.13$ for each chromophore. The SHG performance is thus about 33% of the optimum predicted by Zyss' model but without taking into account the local effect of the J aggregation of the [DAMS$^+$] chromophore, which induces an enhancement of the SHG.[8,20]

In principle, we could not neglect the contribution to the bulk SHG given by DAMBA, a polarizable push−pull molecule itself oriented in a way to give $b_{eff}/\beta_{CT} \sim 0.10$. However, the rather low EFISH[32] value of molecular quadratic hyperpolarizability β (23×10^{-30} esu)[33] would suggest only a minor role of DAMBA. In addition, comparing the crystalline nonlinearity per molecule in **1**−**6** ($b_{eff}/\beta_{CT} = 0.13$) and [DAMS$^+$][*p*-toluenesulfonate] ($b_{eff}/\beta_{CT} = 0.11$), we note that all these materials share a similar SHG efficiency. Therefore, we can conclude that the SHG efficiency can be ascribed almost entirely to the [DAMS$^+$] NLO-phore.

Magnetic Properties. For compounds **1**−**6** the magnetic properties are given by the presence of magnetic ions embedded in the inorganic network (see Figure 3), where the strength of the magnetic interactions between the M(II) and M(III) ions can be tuned also by the insertion of diamagnetic M(II) or M(III) ions in the bivalent and trivalent sites of the polymeric inorganic "stripes". While the magnetic coupling is expected to be weak in the archetypal compound **1** due to the presence of the diamagnetic Rh(III) ion, the insertion of the magnetic Cr(III) and Fe(III) ions in the polymeric inorganic stripes is expected to potentially lead to interesting magnetic properties for compounds **2** and **3**. The validity of this design strategy in order to obtain tunable magnetic properties is further evidenced by the substitution of the Mn(II) by the Zn(II) ion. While compound **4** is diamagnetic, **5** and **6** should show some interaction, though weaker than those of **2** and **3** and in a way somewhat similar to that of compound **1**.

Magnetic measurements were thus performed on polycrystalline materials **1**−**3** and **5**−**6** in the range 2−300 K.

In all investigated compounds the value of the χT product (where χ is the molar magnetic susceptibility and T is the temperature) at high temperature is consistent with what is expected for their crystalline structure. In compound **1** the only magnetic centers are the octacoordinated Mn(II) ions, being Rh(III) diamagnetic. The high-temperature value, 4.33 emu*K/mol at 300 K, is consistent with the presence of isolated high spin Mn(II) centers ($S = {}^5/_2$, $g = 2.0$) not strongly interacting through the polymeric chains of the inorganic "stripes". The χT value remains almost constant down to 6 K, markedly decreasing only below this temperature. The observed decrease may be due to weak antiferromagnetic interactions or to zero-field splitting effects. In the former hypothesis, the weakness of these interactions is consistent with the extremely long distance from one paramagnetic metal center to the other, which consists of one Rh(III) ion and two bridging oxalate ligands (see Figure 3). The Mn(II) ions are connected by two such bridges, equivalent one to the other as each of them is composed by a long and short distance between the M(II) site and the oxalate (see Table 2). The experimental data were fitted by a classical Heisenberg chain model,[34] Mn(II) being an isotropic

(31) The spectroscopic evidence of J aggregation suggests that a non-negligible interchromophoric interaction is taking place. Quantifying the perturbation of such an interaction into Zyss interpretation is an interesting argument that we will discuss in further publication. Nevertheless, we believe that the response obtained by applying this model can be considered at least as a qualitative analysis.

(32) (a) Levine, B. F.; Bethea, C. G. *Appl. Phys. Lett.* **1974**, *24*, 445−447. (b) Singer, K. D.; Garito, A. F. *J. Chem. Phys.* **1981**, *75*, 3572−3580. (c) Ledoux, I.; Zyss, *J. Chem. Phys.* **1982**, *73*, 203−213.

(33) Dulcic, A.; Sauteret, C. *J. Chem. Phys* **1978**, *69*, 3453.

(34) (a) Fisher, M. E. *Am. J. Phys.* **1964**, *32*, 343. (b) Dingle, R.; Lines, M. E.; Holt, S. L. *Phys. Rev.* **1969**, *187*, 643.

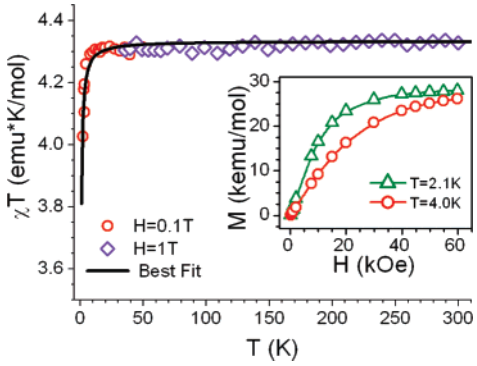

Figure 6. Temperature dependence of the product χT for compound **1**. Points represented as circles were recorded in a static applied field of 1 kOe, while rhombuses, at 10 kOe. The solid line is the best fit to the curve using a Heisenberg chain model, as described in the text. In the inset, magnetization versus field curves are reported for two temperatures: 2.1 and 4.0 K.

ion with a high ground spin state. The Hamiltonian $\mathscr{H}$ we considered has the form:

$$\mathscr{H} = -\sum_{i=1}^{N}(JS_iS_{i+1} + \mu_B S_i\, gH) \qquad (3)$$

where J is the exchange interaction, S_i, the spin coordinates at the i-th site of the chain, g, the Landé factor, μ_B, the Bohr magneton, and H, the externally applied magnetic field. The summation over the i index runs all over the N chain sites. For large N, i.e., in the limit of an almost infinite chain, and since the high spin Mn(II) centers, having $S = {}^5/_2$, can be represented as classical spin vectors, the Hamiltonian (eq 3) leads to a conveniently compact expression that allows fitting of the data for the molar susceptibility according to eq 4:

$$\chi T = \frac{g^2\beta^2 S(S+1)}{3k_B}\frac{1+u}{1-u} \qquad (4)$$

where $\beta = (k_B T)^{-1}$ and $u = \coth[\beta JS(S+1)] - [\beta JS(S+1)]^{-1}$. The simulation gives good agreement between the theoretical curve and the experimental data (agreement factor $R = 0.9915$). The best-fit values were found to be $J/k_B = -0.023 \pm 0.002$ K and $g = 2.00 \pm 0.05$, as expected for such a long interaction pathway.[35] Magnetization versus field measurements performed at 2.1 and 4.0 K, shown in the inset of Figure 6, also gives a saturation value of 5.04 μ_B, again in agreement with a very weak interaction of the Mn(II) ions.

The dramatic effect of the substitution of the diamagnetic Rh(III) ion by a M(III) magnetic center is clearly visible in Figure 7, where the temperature dependence of the χT curve is reported for compound **3** containing the Cr(III) ion. As in the previous case, we have found a high-temperature value (8.2 emu*K/mol at 300 K) in good agreement with both the crystal structure and the theoretical value calculated considering the presence of two Cr(III) ions, $S = {}^3/_2$, and one Mn(II) ion, $S = {}^5/_2$, in every monomeric unit of the polymeric chain of an

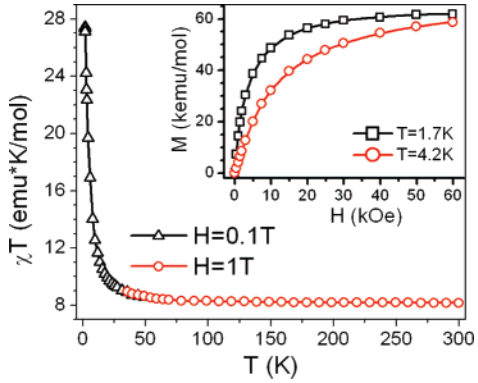

Figure 7. Temperature dependence of the product χT for compound **3**. Points represented as triangles were recorded in a static applied field of 1 kOe, and those represented as circles, at 10 kOe. In the inset, magnetization versus field curves are reported for two temperatures: 1.7 and 4.2 K.

inorganic "stripe". This structure is an example of a spin staircase system, and the χT product smoothly increases as the temperature is lowered,[35] according to the presence of dominant ferromagnetic interactions. This coupling, mediated by the oxalate bridges between the two different metal ions, is much stronger (about 1 order of magnitude) than the antiferromagnetic interaction between the isolated Mn(II) centers in agreement with all the examples of Cr(III) and Mn(II) ions interacting via oxalate bridges reported in the literature.[36] It is apparent that the octacoordination around manganese(II) does not dramatically alter the mechanism of the exchange pathways. An estimate of the strength of the coupling interaction was obtained from a fit with the Curie−Weiss law of high-temperature data (R = 0.999 91) and gave a ferromagnetic value of $J = 3.23 \pm 0.04$ K. Magnetization versus field measurements performed at 1.7 and 4.2 K, shown in the inset of Figure 7, gave a magnetization saturation value of 11.09 μ_B, as expected for the presence of one Mn(II) and two Cr(III) ions interacting by a ferromagnetic process. Saturation was reached at lower field values than those for compound **1**, confirming a ferromagnetic behavior.

The Fe(III)-containing compound, **2**, shows a temperature dependence of the χT product (Figure 8) that is a clear indication of a one-dimensional material with no appreciable three-dimensional long-range ordering.[37] At high temperature the χT value (12.8 emu*K/mol at 300 K) is slightly lower than expected (13.125 emu*K/mol) for one high spin Mn(II) ion and two high spin Fe(III) ions per repeating unit which are uncoupled. Contrary to **3**, the Cr(III) containing material, the χT curve of **2** decreases steadily on lowering the temperature and reaches a minimum at 25 K (χT being 7.9 emu*K/mol), where a marked increase of the susceptibility gives rise to a sharp peak at 10 K (χT being 14.8 emu*K/mol) in $H = 1$ kOe. Such behavior is quite typical of ferrimagnetic systems.[38] The field dependence of χT is due to saturation effects. Zero-field-cooled and field-

(35) (a) Willett, R. D.; Galeriu, C.; Landee, C. P.; Turnbull, M. M.; Twamley, B. *Inorg. Chem.* **2004**, *43*, 3805. (b) Dagotto, E.; Rice, T. M. *Science* **1996**, *271*, 618. (c) Dagotto, E. *Rep. Prog. Phys.* **1999**, *62*, 1525. (d) Barnes, T.; Dagotto, E.; Riera, J.; Swanson, E. S. *Phys. Rev. B* **1993**, *47*, 3196. (e) Mayaffre, H.; Auban-Senzier, P.; Nardone, M., Jérome, D.; Poilblanc, D.; Bourbonnais, C.; Ammerahl, U.; Dhalenne, G., Revcolevschi, A. *Science* **1998**, *279*, 345.

(36) (a) Ohba, M.; Tamaki, H.; Matsumoto, N.; Okawa, H. *Inorg. Chem.* **1993**, *32*, 5385. (b) Tamaki, H.; Zhong, Z. J.; Matsumoto, N.; Kida, S.; Koikawa, M.; Achiwa, N.; Hashimoto, Y.; Okawa, H. *J. Am. Chem. Soc.* **1992**, *114*, 6974. (c) Kahn, O. *Acc. Chem. Res.* **2000**, *33*, 648. (d) Kahn, O.; Pei, Y.; Verdaguer, M.; Renard, J. P.; Sletten, J. *J. Am. Chem. Soc.* **1988**, *110*, 782. (e) Lloret, F.; Nakatani, K.; Journaux, Y.; Kahn, O.; Pei, Y.; Renard, J. P. *J. Chem. Soc., Chem. Commun.* **1988**, 642. (f) Delhaes, P.; Koningsbruggen, P. J.; Kahn, O.; Nakatani, K.; Pei, Y.; Renard, J. P.; Drillon, M.; Legoll, P. *Inorg. Chem.* **1990**, *29*, 3325. (g) Kahn, O. In *Organic and Inorganic Low DimentionaI Crystalline Materials*; Drillon, M., Ed.; NATO AS1 Series 168; Plenum: New York, 1987; p 93.

(37) Carlin, R. L. *Magnetochemistry*; Springer-Verlag: New York, 1986.

(38) Lescouezec, R.; Vaissermann, J.; Toma, L. M.; Carrasco, R.; Lloret, F.; Julve, M. *Inorg. Chem.* **2004**, *43*, 2234.

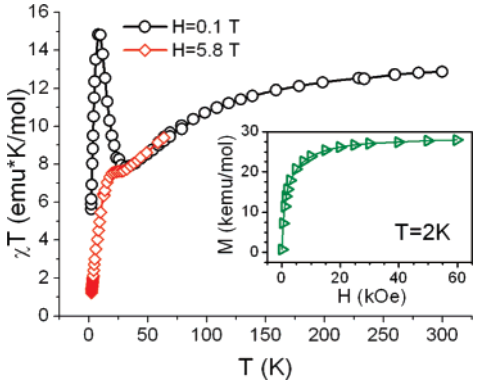

Figure 8. Temperature dependence of the product χT for compound **2**. Points represented as black circles were recorded in a static applied field of 1 kOe, and those represented as smaller red rhombuses, at 58 kOe. In the inset, the magnetization versus field curve is reported at 2 K.

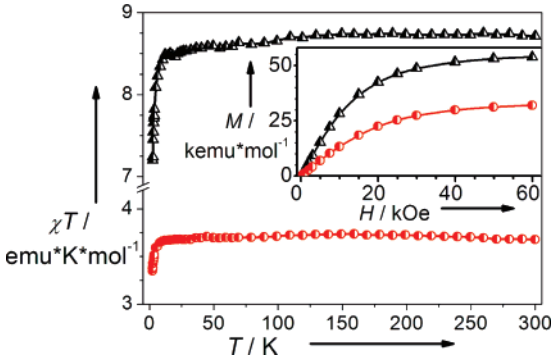

Figure 9. Temperature dependence of the product χT for compounds **5** (triangles) and **6** (circles). All data were recorded in a field of 10 kOe. In the inset magnetization versus field curves are reported for both compounds **5** (triangles) and **6** (circles), as recorded at 2.5 K.

cooled measurements revealed no sign of irreversibility, thus further confirming the absence of long-range 3D ordering due to interchain interactions. The magnetization curve as a function of the field, recorded at 2.0 K, shown in the inset of Figure 8, gave a saturation value of 5.03 μ_B, in agreement to what is theoretically predicted for a single $S = {}^5/_2$ ion with $g = 2$. This value can be explained with the presence of two Fe(III) ions oriented parallel to each other and antiferromagnetically coupled to the alternating Mn(II) ions, to give a ferrimagnetic state. Therefore, consistent with this ferrimagnetic behavior, the magnetic structure of the polymeric inorganic chain of **2** at low temperature can be schematized with the magnetization of Mn(II) ions opposed to that of both of the alternating Fe(III) ions. A high-temperature fit of the data with the Curie−Weiss law ($R = 0.999\,94$) revealed a significant, antiferromagnetic coupling, estimated as $J = -34.5 \pm 0.2$ K. This rather high value is in overall agreement with what was previously reported for similar compounds.[36]

Both compounds **5** and **6** were found to display, at best, a weak antiferromagnetic coupling, as reported in Figure 9. In the case of the Fe(III)-containing compound **5** a $\chi T = 8.7$ emu*K/mol value is reached at 300 K, consistent with the presence of two high-spin Fe(III) magnetic centers in each repeating unit of the "stripe". As can be noticed from the curve of Figure 9 (black triangles) the magnetic Fe(III) centers are only weakly antiferromagnetically coupled, according to a χT value that decreases very slightly down to 12 K, markedly showing the effect of interactions only below this temperature.

Table 3. Magnetic Behavior of the $[DAMS]_4[M(III)_2M(II)(C_2O_4)_6]\cdot 2DAMBA\cdot 2H_2O$ **1**−**6** Compounds

compound	coupling	M_{sat} at 2 K (μ_B)	coupling constant
1	weak antiferromagnetic	5.04	$J = -0.023 \pm 0.002$ K
2	ferrimagnetic	5.03	$J = -34.5 \pm 0.2$ K
3	ferromagnetic	11.09	$J = 3.23 \pm 0.04$ K
5	weak antiferromagnetic	9.64	$J = -1.0 \pm 0.1$ K
6	weak antiferromagnetic	5.75	$J = -0.7 \pm 0.1$ K

As no effect of the growth of the correlation length is visible from the χT plot, the magnetic interaction pathway, responsible for the decrease of the χT value, can be due to either antiferromagnetic coupling between the two Fe(III) centers of the same repeating unit or that between Fe(III) centers placed in two adjacent monomeric units. A Curie−Weiss plot ($R = 0.999\,99$) revealed that these interactions ($J = -1.0 \pm 0.1$ K) are more than 1 order of magnitude stronger than those between Mn(II) centers, for instance in compound **1**, but considerably lower than those obtained for **2** and **3** when both M(II) and M(III) centers are magnetic. The presence of only weak interactions is also revealed by the magnetization vs field curve, reported in the inset of Figure 9, which is in agreement with the presence of two very weakly coupled Fe(III) centers, as the saturation value of 9.64 μ_B is reached at 60 KOe.

The Cr(III)-containing compound **6** shows a similar behavior: a $\chi T = 3.68$ emu*K/mol value is reached at 300 K, in agreement with the presence of two Cr(III) magnetic centers in each repeating unit of the polymeric chain. From the curve of Figure 9 (half-filled circles) it appears that the Cr(III) centers are coupled by weak antiferromagnetic interactions, whose effect is clearly visible only below 10 K. Again no effect of the growth of the correlation length is visible in the temperature range accessible to us, and no guesses can be made on the precise interaction pathway responsible for the decrease of the χT value, which could be due to either coupling between Cr(III) centers in the same repeating unit or that in two adjacent monomeric units. Linear regression performed on a Curie−Weiss plot in the temperature region between 50 and 300 K ($R = 0.999\,94$) revealed that these interactions ($J = -0.7 \pm 0.1$ K) are weaker than those in compound **5** but stronger than those between Mn(II) centers, for instance in compound **1**, but extremely lower than those obtained in compounds **2** and **3** containing magnetic M(II) and M(III) centers. The magnetization vs field curve, reported in the inset of Figure 9, is in agreement with the presence of two very weakly coupled Cr(III) centers, and the saturation value of 5.75 μ_B is reached at a field of 60 kOe.

In Table 3 we have summarized the main magnetic properties of compound **1**−**6** in order to show the extreme flexibility of the tunability of the magnetic properties in these materials, characterized mainly by 1D magnetic interaction along the polymeric chains of the inorganic "stripes" of the crystalline network.

Conclusions

In this work, we reported the preparation as well as X-ray structural and magnetic characterization together with the evidence of a very large solid-state SHG of a new family of hybrid inorganic−organic layered crystalline materials, based

on mixed M(II)/M(III) (M(II) = Mn, Zn; M(III) = Rh, Cr, Fe) oxalates and the efficient second-order NLO-phore [DAMS$^+$].

These hybrid materials are characterized by an unusual crystalline network. A 2D layer contains the inorganic part, formed by infinite "stripes" of polymeric mixed M(II)/M(III) metal oxalates linked by hydrogen bonds through DAMBA and water molecules. The *para*-dimethylaminobenzaldehyde plays a rather unique role because it stabilizes the organic−inorganic layer and therefore induces the segregation of second-order NLO-phores, [DAMS$^+$], in layers of self-organized head-to-tail J aggregates. The origin of this peculiar organic−inorganic layer is due to the connection of the metals to three and four oxalates (M(III) and M(II), respectively, in a 2:1 ratio) that produces 1D "stripes" instead of the more common honeycombs.[29] M(III) ions display a typical hexacoordination, whereas M(II) ions are tetra- or (strongly asymmetrically) octacoordinated.

Conditions to stabilize ordered layers of head-to-tail cationic organic second-order NLO-phores, arranged as J aggregates, are not easily predicted. In the literature few hybrid inorganic−organic materials have been reported containing organic NLO-phores as ordered layers controlled by either an inorganic-only[8,10,20] or by a "solvent-templated" inorganic network.[39]

The main properties of the new materials reported here are the very large SHG (same order of magnitude of the highest values for materials containing the same organic NLO-phore reported so far)[8,14] and the interesting tunability of the magnetic ordering, obtained by choosing the proper pair of M(II)/M(III) ions. For example, the interaction between magnetically active Mn(II) ions is rather weak in combination with the diamagnetic Rh(III) ions, but it is more relevant if associated with Cr(III) or Fe(III) ions (with ferri- or ferromagnetic nature, respectively). The weak antiferromagnetic interactions characterizing compounds **1**, **5**, and **6** as well as the stronger magnetic interactions of compounds **2** and **3** reveal that the spin-staircase systems of this class of mixed oxalates can be adequately described by nontrivial next-nearest interactions along the M(II)/M(IIII) ions of the polymeric chains of the inorganic "stripes". Since the magnetic interactions seem to occur mainly along the polymeric chain of these "stripes" we may have in the crystalline network an anisotropy of the magnetic behavior. In order to confirm the evidence of preferential magnetic interactions along each 1D inorganic "stripe" and not between two adjacent ones, we plan to perform accurate magnetic measurements on oriented single crystals.

The very large second-order NLO response is originated by (a) the significant molecular quadratic hyperpolarizability of the [DAMS$^+$] NLO-phore; (b) their ordered self-organization within the intercalated organic layers; and (c) their efficient J type aggregation,[21] which is in fact known to increase the second-order NLO response.[8,20] Although a direct relationship between the second-order NLO properties and the 1D magnetic structure cannot be established, we note that the magnetic shielding of the "stripes", due to the organic bridge of DAMBA and the intercalation of NLO-phores layers, is extremely efficient in lowering 2D and 3D magnetic interactions and ordering. This seems to facilitate 1D anisotropic magnetic interactions, a subject which has recently attracted considerable interest.[40]

In conclusion, both the very large SHG and the 1D anisotropic magnetic interactions allow us to classify the materials investigated here as a new class of polyfunctional hybrids, totally different with respect to the more common mixed M(II)/M(III) honeycomb layered metal oxalates.[10]

Because the research on hybrid inorganic−organic materials is moving toward increasing the transparency/nonlinearity trade-off, at the expense of SHG efficiency,[41,42] we plan to investigate the same inorganic framework coupled with more transparent NLO-phores.

Acknowledgment. This work was supported by the Ministero dell'Istruzione, dell'Università e della Ricerca (Research Program FIRB, year 2003, Research Title "Molecular compounds and hybrid nanostructured materials with resonant and non-resonant optical properties for photonic devices"; Research Program PRIN, year 2005, Research Title "Progettazione ed auto-organizzazione di architetture molecolari per nanomagneti e sistemi optoelettronici: Nanoorganizzazione di cromofori per materiali per ottica nonlineare del secondo ordine") and by the Fondazione Cariplo (Bando 2005, Research Title "Nuovi materiali con nanoorganizzazione di cromofori in sistemi Host−guest o su scaffold inorganico per dispositivi fotoluminescenti o optoelettronici").

Supporting Information Available: Curie−Weiss law plots for **2** and **3** and $[DAMS]_4[Cr_2Mn(C_2O_4)_6]\cdot 2DAMBA\cdot 2H_2O$; crystallographic information files (CIF) for **1**, **2**, **3**, and **10**. This material is available free of charge via the Internet at http://pubs.acs.org.

JA0710712

(39) Guloy, A. M.; Tang, Z.; Miranda, P. B.; Srdanov, V. I. *Adv. Mater.* **2001**, *13*, 833−837.

(40) (a) Caneschi, A.; Gatteschi, D.; Lalioti, N.; Sangregorio, C.; Sessoli, R.; Venturi, G.; Vindigni, A.; Rettori, A.; Pini, M. G.; Novak, M. A. *Angew. Chem., Int. Ed.* **2001**, *40*, 1760. (b) Clerac, R.; Miyasaka, H.; Yamashita, M.; Coulon, C. *J. Am. Chem. Soc.* **2002**, *124*, 12837. (c) Lescouezec, R.; Vaissermann, J.; Ruiz-Perez, C.; Lloret, F.; Carrasco, R.; Julve, M.; Verdaguer, M.; Dromzee, Y.; Gatteschi, D.; Wernsdorfer, W. *Angew. Chem., Int. Ed.* **2003**, *42*, 1483. (d) Liu, T.-F.; Fu, D.; Gao, S.; Zhang, Y.-Z.; Sun, H.-L.; Su, G.; Liu, Y.-J. *J. Am. Chem. Soc.* **2004**, *125*, 13976. (e) Pardo, E.; Ruiz-Garcia, R.; Lloret, F.; Faus, J.; Julve, M.; Journaux, Y.; Delgado, F.; Ruiz-Perez, C. *Adv. Mater.* **2004**, *16*, 1597. (f) Ferbinteanu, M.; Miyasaka, H.; Wemsdorfer, W.; Nakata, K.; Sugiura, K.-i.; Yamashita, M.; Coulon, C.; Clerac, R. *J. Am. Chem. Soc.* **2005**, *127*, 2090.

(41) Kotler, Z.; Hierle, R.; Josse, D.; Zyss, J.; Masse, R. *J. Opt. Soc. Am. B* **1992**, *9*, 534.

(42) Horiuchi, N.; Lefaucheux, F.; Ibanez, A.; Josse, D.; Zyss, J. *J. Opt. Soc. Am. B* **2002**, *19*, 1830.